Operating conditions and thermodynamic bounds of dual radiative heat engines

Julien Legendre, Pierre-Olivier Chapuis

Operating conditions and thermodynamic bounds of dual radiative heat engines

Julien Legendre and Pierre-Olivier Chapuis
Univ Lyon, CNRS, INSA-Lyon, Université Claude Bernard Lyon 1, CETHIL UMR5008, F-69621, Villeurbanne, France
(Dated: October 10, 2024)

We propose a unified description of dual radiative heat engines (RHEs), consisting of two facing optoelectronic components (diodes) and capable of generating electrical power from heat. They can operate in three regimes depending on the applied biases, namely in thermoradiative-negative electroluminescent (TRNEL), thermoradiative-photovoltaic (TRPV) or thermophotonic regimes (TPX, consisting of a light-emitting diode and a PV cell). They have access to operating conditions that are unachievable by single RHEs such as thermophotovoltaic systems: at the radiative limit, TRNEL devices can reach the Carnot efficiency for any bandgap, while TPX devices achieve large power outputs by means of electroluminescent enhancement. Expressions of the maximum power output and related efficiency achieved by dual engines are derived analytically, and reveal that the power output of TPX engines is not bounded. A comparison to usual efficiency bounds also highlights the impact of thermalisation losses, and the subsequent interest of spectral filtering to extend the operating region. The influence of nonradiative recombinations is also investigated. This work provides common framework and guidelines for the study of RHEs, which represent a promising solution for reliable and scalable energy conversion.

The conversion of heat into electrical power by means of solid-state heat engines [1], such as thermoelectric [2] and thermionic generators [3], have gathered sizeable attention in the past decades due to their reliability and scalability. These engines also include optoelectronic systems, the most popular ones probably being photovoltaics (PV) for solar application, and thermophotovoltaics (TPV) [4–7]. In the latter case, the radiation comes from a hot emitter maintained at a high temperature by the heat supplied to the system. This gives access to a broad range of applications, for instance in latent heat TPV batteries [8]. But apart from PV and TPV, other optoelectronic systems are able to convert heat into electricity. One is the thermoradiative (TR) cell: as opposed to the PV cell, it is able to generate electrical power by emitting negative electroluminescent radiation to the cold surroundings [9, 10] (e.g. the night sky, outer space) or towards a cold absorber [11]. TR cells, along with PV and TPV cells, are single radiative heat engines: they are heat engines in which one active component produces electrical power either by emitting or absorbing radiation [12]. Their typical electrical characteristic is provided in Section I of Supp. Mat. [13].

It is also possible to couple two different optoelectronic components into a dual radiative heat engine (see Fig. 1). One such dual engine is the thermoradiative-photovoltaic (TRPV) device [14, 15], in which a hot TR cell is coupled to a cold PV cell: both components are then able to generate electrical power, although production by the TR cell limits its emission due to negative electroluminescence, and therefore reduces the PV cell production. Nonetheless, having two components provides better control of the operating conditions. Thermophotonics (TPX) [16–18] has also gathered interest recently. In such a device, the hot emitter is a light-emitting diode (LED). While an LED consumes electrical power, it can emit electroluminescent radiation towards the PV cell with an above-unity wall-plug efficiency (i.e. emitting more power than what it consumes), enabling a significant increase in power output [19]. Recently, TPX devices have mostly been studied in near-field operation, as near-field radiation further increases the power output [20, 21] and limits the impact of non-radiative losses [22].

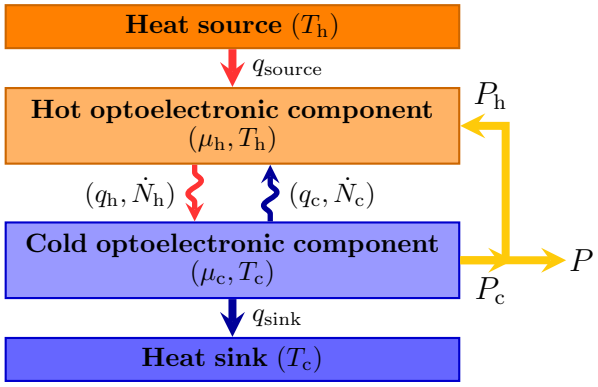

FIG. 1: Representation of the dual radiative engine (here in a thermophotonic configuration). It consists of two optoelectronic components which exchange electroluminescent radiation. By thermally connecting them to a heat source and a heat sink, the heat supplied can be converted into electrical power.

Although the aforementioned systems are all radiative heat engines and share the same core physical laws, they are studied independently of one another in the literature. In this letter, we provide a unified overview of the performance of dual radiative engines, for which every device previously mentioned corresponds to a specific operating regime. It highlights the respective merits of

each engine, and provides a fair comparison of their performance. It also clarifies their capabilities in comparison to single radiative engines. We particularly focus on the maximum achievable power and efficiency, for which we are able to derive closed-form expressions. The comparison to usual limits reveals the significant influence of thermalisation, making spectral filtering an attractive solution to achieve better performances.

In the following, we assume that the dual engine operates in the far field. To maximise the achievable power output, the emission of radiation is assumed to follow the generalised Planck law, which corresponds to the extension of the usual Planck law for non-thermal (here, electroluminescent) radiation [23, 24]. Furthermore, the bandgaps of the two components are assumed to be equal, and the radiation exchanged below the bandgap is neglected to obtain an upper bound of the efficiency. Thus, the emitted photon flux density $\dot{N}$ and the related heat flux density q, respectively expressed in photon and energy per unit time and area, can be expressed as

$$\dot{N}_i = \frac{1}{4\pi^2 c^2 \hbar^3} \int_{E_g}^{\infty} \frac{E^2}{\exp\left(\frac{E-\mu_i}{k_B T_i}\right) - 1} dE, \tag{1a}$$

$$q_i = \frac{1}{4\pi^2 c^2 \hbar^3} \int_{E_g}^{\infty} \frac{E^3}{\exp\left(\frac{E-\mu_i}{k_B T_i}\right) - 1} dE, \tag{1b}$$

where i relates to the emitting body (either "h" or "c") with bandgap energy E_g and temperature T_i. μ_i is the chemical potential of the emitted radiation, which must remain strictly smaller than E_g and is assumed to be related to the voltage U_i applied to the component through $\mu_i = eU_i$ [23, 25, 26], e being the elementary charge. The above integrals can be expressed analytically using polylogarithms [27], leading to

$$\dot{N}_i = \frac{(k_B T_i)^3}{4\pi^2 c^2 \hbar^3} \big(e_{g,i}^2 \,\mathrm{Li}_1(e^{-x_i}) + 2e_{g,i}\,\mathrm{Li}_2(e^{-x_i}) + 2\,\mathrm{Li}_3(e^{-x_i})\big), \tag{2a}$$

$$q_i = \frac{(k_B T_i)^4}{4\pi^2 c^2 \hbar^3} \big(e_{g,i}^3 \,\mathrm{Li}_1(e^{-x_i}) + 3e_{g,i}^2\,\mathrm{Li}_2(e^{-x_i}) + 6e_{g,i}\,\mathrm{Li}_3(e^{-x_i}) + 6\,\mathrm{Li}_4(e^{-x_i})\big), \tag{2b}$$

where Li_n is the n-th order polylogarithm, $e_{g,i} = E_g/k_B T_i$ and $x_i = (E_g - \mu_i)/k_B T_i$. Finally, to obtain an upper bound of the dual engine performance, we assume that any active component operates at the radiative limit (i.e. without any non-radiative losses). The electrical power generated by a component i facing a component j is then

$$P_i = U_i \cdot e(\dot{N}_j - \dot{N}_i) = \mu_i(\dot{N}_j - \dot{N}_i). \tag{3}$$

The total power output is therefore

$$P = (\mu_c - \mu_h)(\dot{N}_h - \dot{N}_c). \tag{4}$$

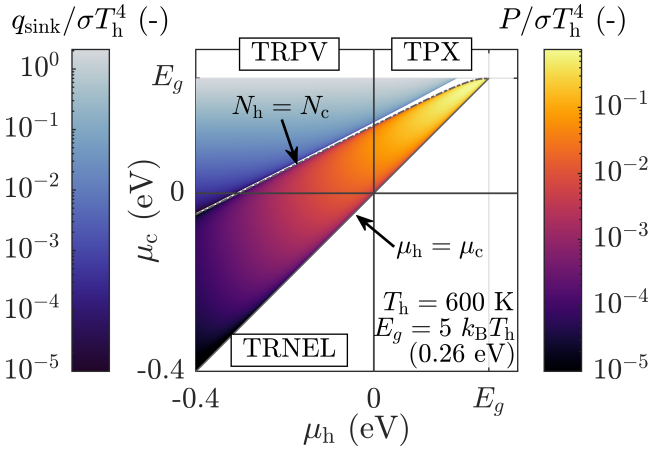

FIG. 2: Performance of dual radiative systems at the radiative limit and for $E_g = 5k_B T_h = 0.26$ eV. This performance is quantified by the electrical power output P for heat engines (central area, right colour scale), and by the heat extracted from the heat sink $q_{sink} = q_h - q_c - P_c$ for heat pumps used for cooling purposes (upper-left area, left colour scale).

Since $q_{source} = q_h - q_c + P_h$, the overall heat engine efficiency is

$$\eta = \frac{P}{q_{source}} = \frac{(\mu_c - \mu_h)(\dot{N}_h - \dot{N}_c)}{q_h - q_c - \mu_h(\dot{N}_h - \dot{N}_c)}. \tag{5}$$

We start by studying how the power output of the dual engine varies in the (μ_h,μ_c) plane. The results obtained considering $T_h = 600$ K and $E_g = 5k_B T_h$ are illustrated in Fig. 2. Although we are mostly interested in heat engine operation, the dual system can also operate as a heat pump [19, 28], and we indicate in a blue colour scale the cooling power. Note that such high cooling powers can only be achieved because below-bandgap radiation is neglected [29].

For the bandgap selected, the dual system is able to operate both as a heat engine and a heat pump in three of the four quadrants: namely, the TPX quadrant ($\mu_h > 0, \mu_c > 0$), the TRPV quadrant ($\mu_h < 0, \mu_c > 0$) but also the "TRNEL" quadrant ($\mu_h < 0, \mu_c < 0$), in which a cold negative electroluminescent (NEL) diode consumes electrical power to limit the radiation sent to the hot facing TR cell. The basic principle of TRNEL operation is similar to that of TPX operation: by supplying one component with electricity, the power generated by the other component get enhanced. The only difference is that TRNEL devices rely on negative (rather than positive) electroluminescence. For more details on TRNEL operation, the corresponding energy diagram can be found in Section I of Supp. Mat. To the best of our knowledge, TRNEL devices have never been mentioned in literature. Going back to Fig. 2, both the power output and the cooling power appear to increase with

μ_c, while P also increases with μ_h: the maximum power point (MPP) is therefore located in the TPX quadrant, while the maximum cooling power is reached in TRPV operation for $\mu_c \to E_g$, where it converges towards a constant value [30]. Additionally, note that for low E_g, the TPX device becomes unable to perform cooling (see Section II of Supp. Mat. [13]).

Note how the dual system does not switch directly from heat engine to heat pump operation as μ varies. Indeed, there is a narrow region in-between where the system is neither able to generate electrical power nor to cool the cold source. This gap can especially be observed when $E_g - \mu_h$ becomes lower than $k_B T_h$, but globally narrows down as the bandgap increases: in the limit of infinite bandgaps, the two operating regions become adjacent as $q_h = q_c$ and $\dot{N}_h = \dot{N}_c$ are equivalent. In this situation, the term related to the lowest-order polylogarithm dominates in the expressions provided in Eq. (2). By linearising Li_1, we obtain that the transition from one region to the other, which corresponds to open-circuit conditions since currents are then equal to zero, occurs approximately for

$$\mu_c = \frac{T_c}{T_h}\mu_h + \left(1 - \frac{T_c}{T_h}\right) E_g + k_B T_c \ln\left(\frac{T_h}{T_c}\right), \qquad (6)$$

this linearised expression being a very good approximation as long as $E_g - \mu_i \gg k_B T_i$. The other side of the power production region is simply delimited by the condition $\mu_h = \mu_c$. These two expressions have already been mentioned for TPX devices in [21].

To quantify and compare the performance of TPX, TRPV and TRNEL devices, we provide in Fig. 3 the $\eta - P$ plots obtained by varying both μ_h and μ_c, considering three different bandgaps and a heat source temperature of 600 K. For each device, the shaded area corresponds to achievable operation, while the full line is the envelope of this area. It is first interesting to notice that while the shape of the admissible $\eta - P$ area changes significantly when considering each engine individually, it remains mostly unchanged with varying bandgaps for the full dual radiative engine. For any of the bandgaps considered, the efficiency at maximum power remains mostly constant (between 28% and 34% of the Carnot efficiency $\eta_C = 1 - T_c/T_h$), while the maximum efficiency is always η_C and is reached at zero power.

If we now compare the different regimes, TRNEL appears to be the one achieving the highest efficiencies. This is enabled by the strong decay of the entropy production when $\mu_{h/c} \to -\infty$, which decreases much faster than the power output. In open-circuit conditions, which are reached roughly for $\mu_h/k_B T_h = \mu_c/k_B T_c$ when $\mu_{h/c} \to -\infty$, this leads the efficiency to reach the Carnot limit. This can be proven using that in such conditions, the ratio $(q_h - q_c)/(\dot{N}_h - \dot{N}_c)$ is independent of the chemical potentials and can thus be neglected in comparison

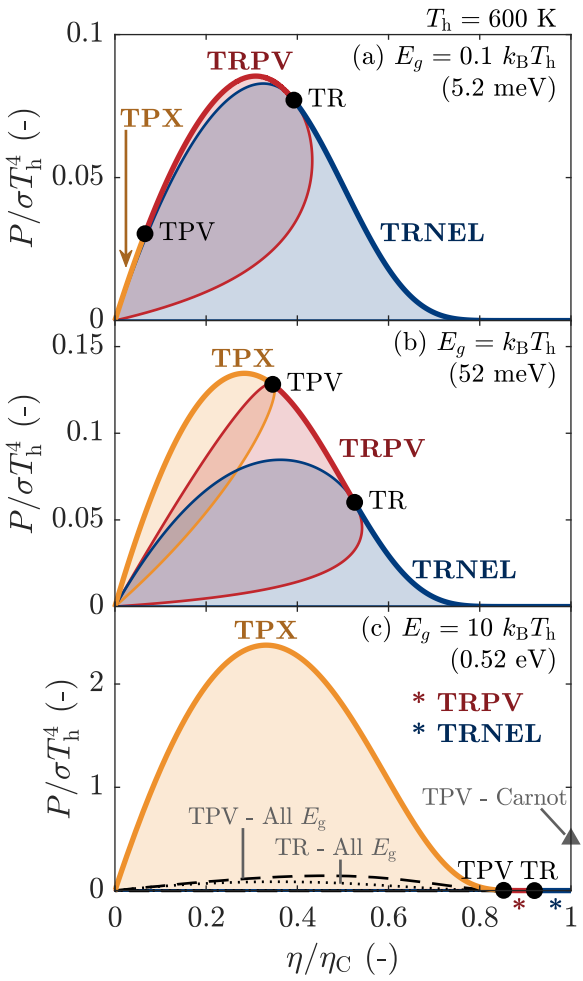

FIG. 3: $\eta - P$ plots of dual radiative engines at the radiative limit, for $T_h = 600$ K and for various bandgaps. The coloured areas represent the $\eta - P$ couples achievable by each dual radiative engine, while the full lines correspond to the envelope of these areas. Power output is normalised by the blackbody emissive power at T_h to make the comparison between systems with different heat source temperatures easier. Efficiency is given relative to the Carnot efficiency: it therefore corresponds to the exergy efficiency or second-law efficiency, and is bounded by one.

to μ_h in Eq. (5). Note that Carnot limit can only be attained because the engine operates at the radiative limit: in Section III of Supp. Mat. [13], we analyse the impact of non-radiative losses on performance by considering a spectrally flat quantum efficiency, and pinpoint that the interest of TRNEL operation vanishes when the quantum efficiency goes significantly below unity. Even at the radiative limit, the advantage of TRNEL operation shrinks for large bandgap: as $E_g \to \infty$, all radiative engines are able to approach the Carnot efficiency in open-circuit conditions. This has already been demonstrated for TR [9, 10] and TPV [31], but can in fact be shown for

any radiative engine. In the limit of an infinite bandgap $(q_\mathrm{h} - q_\mathrm{c})/(\dot{N}_\mathrm{h} - \dot{N}_\mathrm{c}) \to E_g$, leading η to be expressed as $(\mu_\mathrm{c} - \mu_\mathrm{h})/(E_g - \mu_\mathrm{h})$. Using Eq. (6), and keeping in mind that $E_g - \mu_\mathrm{h} \gg k_\mathrm{B}T_\mathrm{h}$, we obtain that the efficiency in open-circuit conditions equals η_C.

To maximise the power output, TPX is almost always the best candidate, TRPV becoming optimal only for very low bandgap energies (here, for $E_g < k_\mathrm{B}T_\mathrm{h} \approx 0.05$ eV) which are difficult to achieve in practice. This remains true for lower or higher heat source temperatures (see Section IV of Supp. Mat. [13]). TPX devices generally outperform other radiative engines in terms of power output because the hot emitter operates as an LED: it is therefore able to largely enhance its emission by electroluminescence, increasing consequently the various energy flows in the system. For high enough bandgaps, this causes P_max to exceed σT_h^4 (see Fig. 3c). This is impossible to reach for single engines, TPV devices generating for instance $P = \eta_\mathrm{C}\sigma T_\mathrm{h}^4$ at most when operating as a Carnot engine and without emitting. Dual engines operating in the TPX regime can therefore largely exceed the power output achieved by single engines for any bandgap (drawn with a dashed line in Fig. 3c). This is one of the main interests of these devices.

While TRNEL devices maximise efficiency and TPX devices power, TRPV systems can in some conditions provide interesting trade-offs between power and efficiency (see Fig. 3b). However, this can only be observed for low bandgaps (a few $k_\mathrm{B}T_\mathrm{h}$ at most) which are hardly achievable for the heat source temperature considered.

The study of $\eta - P$ plots directly highlights that the maximum efficiency of dual radiative engines is always the Carnot efficiency, reached for zero power output. Regarding the MPP, it was observed that P_max increases significantly with E_g while η_MPP varies only slowly, but no analytical expressions of these quantities have yet been formulated. Therefore, in the following, we focus on the analytical derivation of P_max and η_MPP. To do so, we consider once again that $E_g \to \infty$, since this allows reaching the largest possible power output (see Section V of Supp. Mat. [13]). By doing so, the Li_1 term dominates the expressions provided in Eq. (2). The following derivations, which are summarised in Section VI of Supp. Mat. [13], indicates that maximum power output is reached for $\mu_i = E_g - \ln(2)k_\mathrm{B}T_i$, where it is expressed as

$$P_\mathrm{max} = \frac{1}{\hbar}\left(\frac{\ln(2)E_g k_\mathrm{B}(T_\mathrm{h} - T_\mathrm{c})}{2\pi c\hbar}\right)^2. \tag{7}$$

It varies quadratically with the bandgap energy: unlike PV or TPV system, the power output of dual radiative engines is not bounded at the radiative limit. Since there is no optimum bandgap, dual radiative engines are not restricted to mid-infrared bandgaps for low ΔT, and can also be made of near-infrared or visible diodes which typically operate closer to the radiative limit. P_max also depends quadratically on the temperature difference, similarly to thermoelectric engines [32]. These dependences of P_max with E_g and ΔT were already pointed out in [30], although without a complete closed-form expression. Since $E_g \gg k_\mathrm{B}T_i$, both chemical potentials are positive and the maximum power is reached in TPX regime, consistently with the results from Fig. 3.

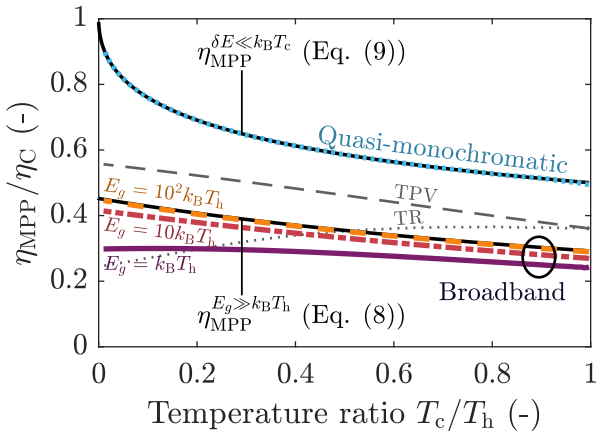

FIG. 4: Variation of the efficiency at maximum power η_MPP with the operating temperature ratio $T_\mathrm{c}/T_\mathrm{h}$. For simplicity, only the TPX quadrant has been considered. The black lines represent the analytical expressions, while the coloured lines correspond to numerical results, either in the quasi-monochromatic case (in blue) or in the broadband case for various bandgaps (from purple to yellow). For comparison, the efficiencies at maximum power achieved by single radiative engines at the optimum bandgap and for broadband radiation are drawn in grey.

The efficiency at maximum power can be written as

$$\eta_\mathrm{MPP}^{E_g \gg k_\mathrm{B}T_\mathrm{h}} = \frac{\eta_\mathrm{C}}{1 + (2 - \eta_\mathrm{C})\chi}, \tag{8}$$

χ being a constant equal to $\frac{1}{2}(\frac{1}{6}(\frac{\pi}{\ln(2)})^2 - 1) \approx 1.21$. The temperature variation of $\eta_\mathrm{MPP}^{E_g \gg k_\mathrm{B}T_\mathrm{h}}$ is provided in Fig. 4 (black line), and matches well the numerical results obtained for bandgaps larger than $100 k_\mathrm{B}T_\mathrm{h}$. It also gives a good estimate of the efficiency obtained for standard bandgaps, as long as $E_g \gg k_\mathrm{B}T_\mathrm{h}$: for $T_\mathrm{h} = 600$ K, $\eta_\mathrm{MPP}^{E_g \gg k_\mathrm{B}T_\mathrm{h}} = 17.7\%$ while $\eta_\mathrm{MPP,1\,eV} = 17.1\%$ and $\eta_\mathrm{MPP,0.52\,eV} = 16.6\%$. In addition, because maximum power diverges when $E_g \to \infty$, below-bandgap radiation would be negligible in comparison to P, being independent of the chemical potential. Consequently, Eq. (8) holds even when below-bandgap radiation is included, and corresponds to the analytical extension of the Shockley-Queisser limit [33] for dual radiative engines.

To better understand how efficient dual radiative engines are at maximum power, one can compare Eq. (8) with classical upper bounds for η_MPP. The Novikov-Curzon-Ahlborn efficiency $\eta_\mathrm{NCA} = 1 - \sqrt{T_\mathrm{c}/T_\mathrm{h}}$ [34, 35]

and the Schmiedl-Seifert efficiency $\eta_{\mathrm{SS}} = 2\eta_{\mathrm{C}}/(4-\eta_{\mathrm{C}})$ [36] are respectively efficiency bounds for endoreversible and exoreversible engines such as thermoelectric generators [37]. For the temperatures previously considered, both efficiencies are close to 29%, hence 11 percent points higher than $\eta_{\mathrm{MPP}}^{E_g \gg k_{\mathrm{B}}T_{\mathrm{h}}}$. This significant difference, which highlights the presence of additional losses in radiative engines, can be attributed to thermalisation losses - i.e., to the fraction of radiative energy exchanged which is useless to optoelectronic conversion. To verify this, we now consider the radiation to be quasi-monochromatic around E_g (i.e. $E_g \leq \hbar\omega \leq E_g + \delta E$ with $\delta E \ll k_{\mathrm{B}}T_{\mathrm{c}}$) so that thermalisation losses become negligible. As demonstrated in Section VII of Supp. Mat. [13], this leads to

$$\eta_{\mathrm{MPP}}^{\delta E \ll k_{\mathrm{B}}T_{\mathrm{c}}} = 1 - \sqrt{\frac{T_{\mathrm{c}}}{T_{\mathrm{h}}}}, \tag{9}$$

exactly the Novikov-Curzon-Ahlborn efficiency. δE being the radiation spectral bandwidth, the maximum power output is then

$$P_{\max} = \frac{1}{\hbar}\left(\frac{E_g\sqrt{k_{\mathrm{B}}}(\sqrt{T_{\mathrm{h}}}-\sqrt{T_{\mathrm{c}}})}{2\pi c\hbar}\right)^2 \delta E, \tag{10}$$

an expression similar to Eq. (7). Since P goes to zero as $\delta E \to 0$, there is a trade-off between power and efficiency as a function of bandwidth, as illustrated in Fig. 5: to achieve non-zero output power, the efficiency must fall below the usual bounds. It is noteworthy that the efficiency starts to decrease for bandwidths as low as few meV (corresponding to a quality factor $Q = E_g/\delta E$ close to 100 for $E_g = 0.52$ eV), while reaching the broadband limit for a bandwidth of few tenths of eV (i.e. for $Q \approx 1$ considering $E_g = 0.52$ eV). If the efficiency at maximum power is too low for a given application, two main leverages are thus available to increase it, although at the expense of power: decrease the radiation bandwidth, or change μ_{h} and μ_{c} to move in the broadband $\eta - P$ plots provided in Fig. 3, which can allow exceeding the aforementioned bounds [7]. The interest of each of these leverages depends on the bandgap, and on how far the system operates from the radiative limit. In some cases, spectral filtering can allow extending the region of achievable operating conditions, limiting the power loss undergone when high efficiency is required (see Section VIII of Supp. Mat [13]).

In conclusion, we have studied the power output and efficiency achievable by dual radiative heat engines, especially when they operate at the radiative limit. This unified description allows shining light on the similarities and respective merits of each operating regime. In particular, TRNEL devices are found to reach Carnot efficiency for any bandgap, while TPX devices are almost always the best dual engines in terms of power output and offer the broadest range of operating conditions for bandgaps over a few $k_{\mathrm{B}}T_{\mathrm{h}}$. In comparison to TPV or TR

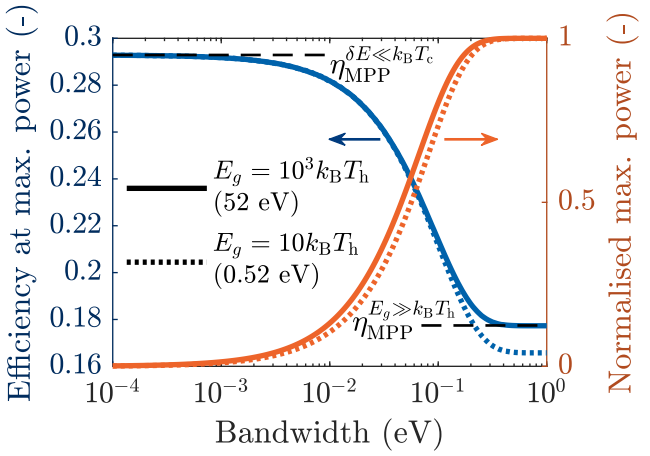

FIG. 5: Variation of the maximum power (in blue) and related efficiency (in orange) for varying spectral bandwidth, considering $T_{\mathrm{h}} = 600$ K. For simplicity, only the TPX quadrant has been considered.

systems, the use of dual engines significantly improves the maximum efficiency of low-bandgap devices and the maximum power of higher-bandgap devices. In addition, we have derived analytical expressions of the maximum power and related efficiency in the $E_{\mathrm{g}} \to \infty$ limit, where power is maximised. This revealed that the maximum power of dual engines is actually not bounded, and that the efficiency is several percent points below usual efficiency limits due to thermalisation losses. Interestingly, spectral filtering can mitigate part of the power loss when high efficiencies are targeted.

The aim of this work was to present the performance of dual radiative engines in a best-case scenario; to model more practical devices, below-bandgap radiation, more advanced models of non-radiative losses and resistive losses shall be included, as well as thermal resistance effects at the thermostats which reduce the operating temperature difference $T_{\mathrm{h}} - T_{\mathrm{c}}$ [26]. In addition, it will be worth investigating how the performance of such engines changes in the near field, where radiative emission exceeds the generalised Planck law [20, 21, 26].

This work has received funding from the European Union's Horizon 2020 research and innovation programme under Grant Agreement No. 951976 (TPX-Power project). The authors thank T. Châtelet, P. Kivisaari, O. Merchiers, J. Oksanen and J. van Gastel.

[1] C. Melnick and M. Kaviany, From thermoelectricity to phonoelectricity, Applied Physics Reviews **6**, 021305 (2019).

[2] X.-L. Shi, J. Zou, and Z.-G. Chen, Advanced Thermoelectric Design: From Materials and Structures to Devices, Chemical Reviews **120**, 7399 (2020).

[3] K. A. Abdul Khalid, T. J. Leong, and K. Mohamed, Review on Thermionic Energy Converters, IEEE Transactions on Electron Devices **63**, 2231 (2016).

[4] T. Burger, C. Sempere, B. Roy-Layinde, and A. Lenert, Present Efficiencies and Future Opportunities in Thermophotovoltaics, Joule **4**, 1660 (2020).

[5] A. LaPotin, K. L. Schulte, M. A. Steiner, K. Buznitsky, C. C. Kelsall, D. J. Friedman, E. J. Tervo, R. M. France, M. R. Young, A. Rohskopf, S. Verma, E. N. Wang, and A. Henry, Thermophotovoltaic efficiency of 40%, Nature **604**, 287 (2022).

[6] E. J. Tervo, R. M. France, D. J. Friedman, M. K. Arulanandam, R. R. King, T. C. Narayan, C. Luciano, D. P. Nizamian, B. A. Johnson, A. R. Young, L. Y. Kuritzky, E. E. Perl, M. Limpinsel, B. M. Kayes, A. J. Ponec, D. M. Bierman, J. A. Briggs, and M. A. Steiner, Efficient and scalable GaInAs thermophotovoltaic devices, Joule **6**, 2566 (2022).

[7] M. Giteau, M. F. Picardi, and G. T. Papadakis, Thermodynamic performance bounds for radiative heat engines, Physical Review Applied **20**, L061003 (2023).

[8] A. Datas, A. López-Ceballos, E. López, A. Ramos, and C. del Cañizo, Latent heat thermophotovoltaic batteries, Joule **6**, 418 (2022).

[9] R. Strandberg, Theoretical efficiency limits for thermoradiative energy conversion, Journal of Applied Physics **117**, 055105 (2015).

[10] A. Pusch, J. M. Gordon, A. Mellor, J. J. Krich, and N. J. Ekins-Daukes, Fundamental Efficiency Bounds for the Conversion of a Radiative Heat Engine's Own Emission into Work, Physical Review Applied **12**, 064018 (2019).

[11] P. Santhanam and S. Fan, Thermal-to-electrical energy conversion by diodes under negative illumination, Physical Review B **93**, 161410 (2016).

[12] E. J. Tervo, E. Bagherisereshki, and Z. M. Zhang, Near-field radiative thermoelectric energy converters: a review, Frontiers in Energy **12**, 5 (2018).

[13] See Supplemental Material for more details on the electrical characteristic of optoelectronic components, on the analytical developments, and on the impact of bandgap, heat source temperature, non-radiative losses and bandgap filtering on dual engines' performance.

[14] T. Liao, Z. Yang, X. Chen, and J. Chen, Thermoradiative–Photovoltaic Cells, IEEE Transactions on Electron Devices **66**, 1386 (2019).

[15] E. J. Tervo, W. A. Callahan, E. S. Toberer, M. A. Steiner, and A. J. Ferguson, Solar Thermoradiative-Photovoltaic Energy Conversion, Cell Reports Physical Science **1**, 100258 (2020).

[16] N.-P. Harder and M. A. Green, Thermophotonics, Semiconductor Science and Technology **18**, S270 (2003).

[17] S. McSherry, T. Burger, and A. Lenert, Effects of narrowband transport on near-field and far-field thermophotonic conversion, Journal of Photonics for Energy **9**, 032714 (2019).

[18] T. Sadi, I. Radevici, B. Behaghel, and J. Oksanen, Prospects and requirements for thermophotonic waste heat energy harvesting, Solar Energy Materials and Solar Cells **239**, 111635 (2022).

[19] P. Santhanam, D. J. Gray, and R. J. Ram, Thermoelectrically Pumped Light-Emitting Diodes Operating above Unity Efficiency, Physical Review Letters **108**, 097403 (2012).

[20] B. Zhao, K. Chen, S. Buddhiraju, G. R. Bhatt, M. Lipson, and S. Fan, High-performance near-field thermophotovoltaics for waste heat recovery, Nano Energy **41**, 344 (2017).

[21] J. Legendre and P.-O. Chapuis, GaAs-based near-field thermophotonic devices: Approaching the idealized case with one-dimensional PN junctions, Solar Energy Materials and Solar Cells **238**, 111594 (2022).

[22] J. Legendre and P.-O. Chapuis, Overcoming non-radiative losses with AlGaAs PIN junctions for near-field thermophotonic energy harvesting, Applied Physics Letters **121**, 193902 (2022).

[23] P. Würfel, The chemical potential of radiation, Journal of Physics C: Solid State Physics **15**, 3967 (1982).

[24] A. De Vos, *Endoreversible Thermodynamics of Solar Energy Conversion* (Oxford University Press, 1992).

[25] W. A. Callahan, D. Feng, Z. M. Zhang, E. S. Toberer, A. J. Ferguson, and E. J. Tervo, Coupled Charge and Radiation Transport Processes in Thermophotovoltaic and Thermoradiative Cells, Physical Review Applied **15**, 054035 (2021).

[26] J. Legendre, *Theoretical and numerical analysis of near-field thermophotonic energy harvesters*, Ph.D. thesis, INSA Lyon, available at `https://theses.fr/2023ISAL0094` (2023).

[27] M. A. Green, Analytical treatment of Trivich-Flinn and Shockley-Queisser photovoltaic efficiency limits using polylogarithms, Progress in Photovoltaics: Research and Applications **20**, 127 (2012).

[28] I. Radevici, J. Tiira, T. Sadi, S. Ranta, A. Tukiainen, M. Guina, and J. Oksanen, Thermophotonic cooling in GaAs based light emitters, Applied Physics Letters **114**, 051101 (2019).

[29] T. Châtelet, J. Legendre, O. Merchiers, and P.-O. Chapuis, Performances of far and near-field thermophotonic refrigeration in the detailed-balance approach, in preparation (2024).

[30] B. Zhao and S. Fan, Chemical potential of photons and its implications for controlling radiative heat transfer, in *Annual Review of Heat Transfer*, Vol. 23 (2020) Chap. 10, pp. 397–431.

[31] B. Roux, C. Lucchesi, J.-P. Perez, P.-O. Chapuis, and R. Vaillon, Main performance metrics of thermophotovoltaic devices: analyzing the state of the art, Journal of Photonics for Energy **14**, 042403 (2024).

[32] Y. Apertet, H. Ouerdane, O. Glavatskaya, C. Goupil, and P. Lecoeur, Optimal working conditions for thermoelectric generators with realistic thermal coupling, EPL (Europhysics Letters) **97**, 28001 (2012), arXiv:1108.6164.

[33] W. Shockley and H. J. Queisser, Detailed Balance Limit of Efficiency of p-n Junction Solar Cells, Journal of Applied Physics **32**, 510 (1961).

[34] I. I. Novikov, Efficiency of an atomic power generating installation, The Soviet Journal of Atomic Energy **3**, 1269 (1957).

[35] F. L. Curzon and B. Ahlborn, Efficiency of a Carnot engine at maximum power output, American Journal of Physics **43**, 22 (1975).

[36] T. Schmiedl and U. Seifert, Efficiency at maximum power: An analytically solvable model for stochastic heat engines, Europhysics Letters **81**, 20003 (2008).

[37] Y. Apertet, H. Ouerdane, C. Goupil, and P. Lecoeur, Irreversibilities and efficiency at maximum power of heat engines: The illustrative case of a thermoelectric generator, Physical Review E **85**, 031116 (2012).